THE JOURNAL OF PHYSICAL CHEMISTRY A

© Copyright 2002 by the American Chemical Society VOLUME 106, NUMBER 13, APRIL 4, 2002

FEATURE ARTICLE

Multidimensional Holography by Persistent Spectral Hole Burning

Alois Renn,[†] Urs P. Wild,[†] and Aleksander Rebane*[,‡]

Physical Chemistry Laboratory of The Swiss Federal Institute of Technology, ETH-Zentrum, CH-8092 Zurich, Switzerland, and Physics Department, Montana State University, Bozeman, Montana 59717

Received: October 15, 2001; In Final Form: January 31, 2002

Persistent spectral hole burning (PSHB) in organic molecules doped in a polymer matrix at low temperatures allows optical recording of information in the dimensions of frequency and time, as well as in space and externally applied electric field. We use this special property to demonstrate new types of holograms, which extend conventional spatial-domain optical data storage into the new dimensions. Basic aspects of recording and playback of holograms by persistent spectral hole burning, including relation between frequency- and time-domain response function, is discussed. This paper is elucidating inherent relations between the time- and frequency-domain versions of PSHB holography. We show that by multiplexing holograms in the frequency dimension, we can store a large number (up to 12 000) of image holograms using a single spectral hole burning sample. In the time domain, we show storage and reproduction of ultrashort time-space images on the scale of $10^{-12}-10^{-13}$ s. Experiments demonstrating unusual hologram properties, such as causality-related asymmetry of diffraction, inversion of time coordinate, and ultrafast processing, are presented.

1. Introduction

In the 1960s and early 1970s, it was often envisioned that emerging techniques of optical holography would take over many functions associated with recording, storing, and processing of information, which have been traditionally performed by electronic devices.[1] Today, however, semiconductor electronics and magnetic storage are still dominating technologies, and one may say that once high promises of optical holography have materialized only to a certain extent. Nevertheless, the idea of holography continues to attract much interest, especially as demands for high-capacity, high-speed storage and processing continue to grow.

There are two reasons holography still stands out as a viable alternative to conventional technology. First, holographic storage is using multiple dimensions, and offers, therefore, a potentially very high capacity, which conventional magnetic and semiconductor memories cannot achieve at present. Second, holographic information may be accessed and processed in parallel, which for conventional devices is another challenging task not realized today. The effect of persistent spectral hole burning (PSHB), which we will be using in this paper, has in that respect several intrinsic advantages, which make it particularly well-suited for holographic applications. To spell out how these advantages occur, let us consider an inhomogeneously broadened absorbing material, such as polymer activated with organic dye molecules at low temperature (similar effects are present in dielectric crystals containing ions of rare earth atoms as well as in some other impurity doped solids). It is well-known that at liquid-helium temperature, the inhomogeneous width of an absorption band may be as much as 10^4-10^6 times broader than the homogeneous line width of a single molecule. Upon illumination, such a medium acts similarly to an ensemble of harmonic oscillators, where each oscillator resonates and, therefore,

[†] The Swiss Federal Institute of Technology.
[‡] Montana State University.

10.1021/jp0138025 CCC: $22.00 © 2002 American Chemical Society
Published on Web 03/13/2002

absorbs light at a slightly different frequency. With the use of optically monochromic illumination, each frequency within the inhomogeneous absorption band can be addressed independently. This means that information may be recorded not only in the dimensions of space but also in the dimension of frequency, effectively increasing the storage capacity by a factor of several thousands. What is even more remarkable is that information may be recorded in the dimension of time. Because a harmonic oscillator's time response and frequency response are intimately related to each other via Fourier transformation, one has free parallel access to the recorded information by simply using the conjoined dimension.

A possibility of time-domain holographic storage using an ensemble of harmonic oscillators was considered theoretically already in 1968.[2] It was not, however, before the effect of PSHB was discovered in 1974[3] that these ideas could be actually implemented in optics. PSHB consists of permanent bleaching of an inhomogeneous absorption band and, through this process, provides a mechanism for persistent storage in the frequency dimension. By illumination with a monochromatic laser, absorption may be bleached in a selected narrow frequency interval, leaving behind a narrow spectral hole or a dip in the absorption profile. This is possible because molecules possess narrow homogeneous resonance absorption lines, called purely electronic zero-phonon lines.[4] The frequency of the zero-phonon line varies randomly from one chromophore to another because of local imperfection of the host solid, which causes the phenomenon of inhomogeneous broadening. A suitable combination of SHB parameters creates a unique situation, which has proven to be extremely useful for optical data storage[5] and especially for holography.[6,7] For example, one 1×1 mm^2 area and 100 μm thick polymer film sample can be used to record thousands of high-resolution image holograms with a minimal amount of cross-talk by simply writing every hologram at a slightly different frequency within an inhomogeneously broadened band.[8] For comparison, recording of an equivalent number of holograms in a photorefractive material is a challenging task, especially because all gratings are sharing essentially the same volume (and dynamic range) of the material.[9] By applying to a hole burning sample an external electric field, it is further possible to shift the frequency of the narrow resonances and thus use the voltage as an additional control parameter.[10] By combining the conventional three spatial dimensions with the several additional dimensions available through SHB, the recording density may theoretically reach 10^{10} bits per λ^3 volume. Let us note that at such high recording density the memory capacity becomes limited by statistical noise caused by a finite number of absorbing chromophores.

Because optics operates at a much higher frequency and may provide a much broader bandwidth than electronics, a large capacity optical memory may be potentially operated at a higher data rate and with a shorter readout latency time than a competing magnetic storage system. In particular, because the frequency dimension is in a unique correspondence with the time dimension via Fourier transformation, it is possible to write and read out data from SHB holographic memory directly as a series of time-domain pulses or images. The relation between frequency domain and time domain is utilized in a method known as time-domain holography.[6,11] An interesting demonstration of this new type of holography is recording and playback of complete time-and-space-domain images or events.[12] Furthermore, some organic SHB materials have a spectral bandwidth exceeding several THz, which allows time-domain holograms to be written and read with ultrashort pulses.[13,14]

The second reason that holography is attractive is because in a hologram the information is distributed over the whole storage medium rather than being permanently attached to any particular spatial location or address. The advantage of such parallel, distributed storage is that it can be used for correlation-based associative recall of information. Parallel read−write and associative recall are particularly instrumental for content-dependent retrieval of information from large databases. SHB has been used to demonstrate error-corrective and associative recall of time-and-space-domain events.[15,16] Time-domain associative recall is possible as long as coherently excited molecules retain the information about the phase of the quantum mechanical wave function. The last circumstance may prove useful in the context of quantum computing, which was also originally proposed to overcome intrinsic limitations of electronics and to improve parallel algorithms.

This paper is organized as follows. In section 2, we discuss the basics of spectral hole burning. We will also introduce some specific practical aspects and requirements for SHB materials used for holography. We illustrate our discussion of organic SHB materials by referring to a model system of chlorin molecules embedded in a polymer film. Besides recording of 2100 spectral holes at temperature $T = 1.7$ K, this material has been used for high-resolution hyperspectral imaging of the sun—a demonstration of application of SHB in astrophysics. We also introduce modulation of spectral holes by Stark shift, which allows an external electric field to be used as an additional storage parameter. We also describe an alternative way of detecting spectral holes by using short laser pulses. The relation between the frequency-domain and time-domain response function of SHB medium is discussed.

Section 3 is devoted to different techniques used for frequency multiplexing in holographic storage. The special role of the hologram phase is elucidated by introducing the technique of frequency and phase swept (FPS) holograms. We use FPS holograms to show new diffraction properties depending on the programmed frequency-phase relation.

In section 4, we discuss the basics of time-domain holographic storage and time-and-space-domain holography of events. We particularly focus on prospective applications of time-domain holography for storage and processing on the time scale of 10^{-12}−10^{-13} s. To achieve the performance on the ultrafast time scale, we again utilize organic dye-doped polymer SHB materials, which are distinguished by having up to 10 THz inhomogeneous bandwidth. We also discuss unusual properties of SHB holograms such as causality-related asymmetry of diffraction and inversion of the time coordinate, ultrafast frequency-domain processing, and associative recall of events. The ultimate advantage of ultrafast holography consists of how a massive amount of data can be addressed and processed in parallel. The holographic method provides a natural way to combine and manipulate different optical degrees of freedom—the three spatial degrees of freedom, the frequency coordinate, and connected to it via Fourier transformation the time coordinate. Time-and-space-domain holography serves as a multispectral generalization of conventional holography.

2. Persistent Spectral Hole Burning

In this paragraph, we will discuss basic properties of spectral hole burning on an example of chlorin (2,3-dihydroporphyrin) molecules. Figure 1a shows the absorption of a chlorin-doped polyvinylbutyral (PVB) film in the spectral region 615−645 nm, corresponding to the electronic transition between the S_0 ground state and the lowest excited singlet electronic state, S_1.

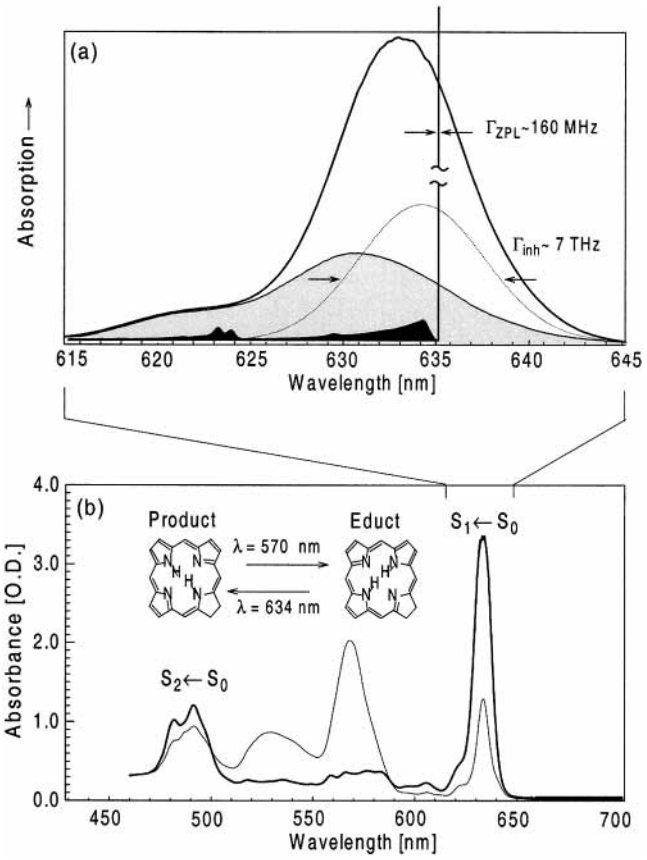

Figure 1. Absorption spectrum and low-temperature phototautomerization of chlorin molecules in PVB at $T = 1.7$ K: (a) internal composition of inhomogeneous absoprtion band of $S_1 \leftarrow S_0$ transition; (b) absorption spectrum of the sample in a broader range of wavelengths before illumination (bold curve) and after illumination (thin curve). Source of illumination was an incandescent lamp combined with an interference filter with 625−645 nm pass band. Insert shows the reversible photochemical reaction responsible for SHB.

At liquid-helium temperature, the homogeneous absorption spectrum consists of a high peak intensity purely electronic zero-phonon line (ZPL, narrow vertical line) and of an accompanying phonon sideband (black area).[4] The sideband incorporates a broad phonon spectrum along with some distinct peaks due to intrinsic vibrations of the molecule. The Debye−Waller factor, α_{DW}, is defined as the ratio between the integrated intensity of the ZPL and the overall integrated intensity of the homogeneous spectrum and characterizes the coupling between the electronic transition and the vibrational modes. In this regard, the ZPL is analogous to the narrow γ-resonance line observed in Mössbauer spectroscopy. In our present optical spectrum, $\alpha_{DW} \approx 0.7$ at $T = 2$ K, and decreases rapidly with increasing temperature, which is characteristic of disordered solids such as polymers and glasses. In Figure 1, the homogeneous ZPL line width is shown to be $\Gamma_{ZPL} \approx 160$ MHz at $T = 2$ K. At even lower temperatures, the ZPL width decreases approximately as $T^{1.3}$, and at few tens of millikelvin, it starts to approach the limiting value, $\Gamma_{ZPL} \approx 20$ MHz, given by fluorescence lifetime of chlorin in PVB, $\tau_f \approx 8$ ns.[17]

The inhomogeneous absorption spectrum (bold curve) can be obtained from the homogeneous spectrum by convolution with a bell-shaped inhomogeneous distribution function (dashed curve). The width of the inhomogeneous distribution is in the present case about $\Gamma_{inh} \approx 7$ THz (230 cm^{-1}). The shaded area shows which part of the total absorption is the contribution from the nonselective part of the spectrum, that is, from phonon sidebands and vibrational lines.[18] The rest (unshaded) of the area corresponds to the absorption by the ZPLs. The ratio between the inhomogeneous and homogeneous line width is $\Gamma_{inh}/\Gamma_{ZPL} = 4 \times 10^5$.

In general, spectral hole burning (SHB) consists of depleting the absorption at one selected frequency within the inhomogeneous band. Depending on the mechanisms involved, such change of absorption may be either short-lived (transient SHB) or permanent (persistent SHB). Transient hole burning occurs whenever the rate of excitation from the ground state to the excited state exceeds the rate of repopulation of the ground state. Transient hole burning may be achieved in many different types of absorption spectra, especially if one uses a sufficiently intense source of monochromatic excitation. Therefore, transient SHB has many known examples in electronic transitions in the visible- and near-IR range, in rotational−vibrational transitions in mid-IR, as well as in radio frequency NMR/EPR spectra. However, as soon as the monochromatic source is switched off, the system rapidly returns to its initial equilibrium population distribution. In contrast, PSHB requires that the system will *not* return to the equilibrium, at least for a time that is longer than the time scale of the experiment. To achieve a permanent spectral transformation, we use a photochemical reaction at low temperature, called phototautomerization, known to occur in many free-base tetrapyrrolic pigments including chlorin. Figure 1b shows spectral transformation of chlorin-doped PVB at low temperature. If the sample is first cooled from room temperature, then the $S_1 \leftarrow S_0$ transition band is centered at 635 nm. By illuminating the sample at 635 nm, the intensity of the 635 nm band decreases, while absorption of product $S_1 \leftarrow S_0$ transition at 570 nm increases. The insert shows that the tautomerization reaction consists of switching the position of two central protons inside the pyrrolic ring of the molecule. In chlorin, educt and product of this reaction are both quite stable at low temperature, and one can have spectral holes with a practically unlimited lifetime, at least as long as low temperature is maintained.

In addition to tautomerization, several other photochemical reactions leading to formation of long-lived spectral holes have been studied in organic molecules. Nonphotochemical hole burning is observed if absorption results in rearranging the local surrounding of the molecule in a way that shifts the ZPL frequency by an amount much larger than Γ_{ZPL} but still smaller than Γ_{inh}. Let us mention that in rare earth ions, such as Pr^{3+}- and Eu^{3+}, doped into inorganic crystals, such as Y_2SiO_5 and $YAlO_3$, long-lived spectral holes are observed by virtue of metastable hyperfine levels in the ion's ground state.[19,20] For a review of different SHB mechanisms, see ref 21 and references therein.

2.1. Detection of Spectral Holes in Frequency Domain. Consider a plate of thickness d composed of a resonantly absorbing inhomogeneously broad material, similar to that shown in Figure 1a. The coefficient of absorption is given by convolution of two functions:

$$\alpha(\nu,z) \propto \int_{-\infty}^{\infty} g(\nu',z)\Gamma(\nu' - \nu)\, d\nu' \qquad (1)$$

where $\Gamma(\nu)$ is molecule's homogeneous line shape (assumed to be the same for all molecules), $g(\nu,z)$ is inhomogeneous distribution of the ZPL frequency, and z is the distance from the front surface of the sample. Prior to illumination, the inhomogeneous distribution is the same for all locations inside the sample and is usually defined by a smooth, broad bell-shaped function, $g(\nu,z) = g_0(\nu)$. Now assume that the medium is

illuminated with a stationary light source with a spectral intensity function, $I_L(\nu)$. Then, at time t after the illumination began, the number of molecules is decreasing at a rate proportional to[22]

$$\frac{dg(\nu,z,t)}{dt} \propto -\eta\, e^{-\int_0^z \alpha(\nu,z')\,dz'}\, g(\nu,z,t) \int_{-\infty}^{\infty} I_L(\nu')\Gamma(\nu'-\nu)\,d\nu' \tag{2}$$

where η is the probability of photochemical transformation. Solving of these equations requires, in general, an extensive numerical computation. However, in case of a monochromatic light source with a frequency ν_0, $I_L(\nu) = I_L\delta(\nu - \nu_0)$, small optical density of the medium, $\alpha(\nu)d \leq 1$, and shallow depth (small contrast) of a spectral hole, $\Delta g < g_0$, it can be shown that the change of the inhomogeneous distribution function is simply proportional to the homogeneous spectrum of the molecules:

$$\Delta g(\nu) \propto \Gamma(\nu - \nu_0) \tag{3}$$

Furthermore, in the experiments described in this paper, the Debye−Waller factor is quite large, $\alpha_{DW} > 0.5$, and we can assume that the phonon sideband is small compared to the ZPL. In this case, the change of the absorption coefficient can be readily expressed as

$$\Delta\alpha(\nu) \propto \gamma(\nu) \tag{4}$$

where

$$\gamma(\nu) = \frac{(2\Gamma_{ZPL})^2}{(\nu - \nu_L)^2 + (2\Gamma_{ZPL})^2} \tag{5}$$

is a Lorentzian resulting from convolution of the homogeneous ZPL line shape with itself. According to this simple description, a nonsaturated spectral hole burned with a monochromatic laser in a sample that has low optical density is an almost perfect "negative" image of the homogeneous ZPL line shape. If the illumination is performed at more than one frequency, then, in the same approximation, the change of the absorption coefficient is given by

$$\Delta\alpha(\nu) \propto \int_{-\infty}^{\infty} I_L(\nu')\gamma(\nu'-\nu)\,d\nu' \tag{6}$$

In other words, in the simplest possible case considered throughout this paper, the spectral profile of the holes is given by convolution of the spectral intensity distribution of the illuminating light with a narrow Lorentzian.

Figure 2 shows the absorbance of a chlorin-doped PVB at temperature $T = 2.0$ K, in which we have burned a large number of narrow spectral holes.[23] Prior to the illumination, the spectrum had a smooth profile with a maximum optical density OD = 1.0. The thickness of the PVB film was $d = 0.2$ mm. Spectral holes were burnt by tuning the frequency of a single-mode dye laser ($\Delta\nu_L < 1$ MHz) in small steps of 3.1 GHz (0.003 nm), starting from the high-frequency side of the band. Because of a peculiarity of the scanning mechanism of the laser, the holes are clustered in seven groups, each group comprising 300 holes. The total number of the holes burnt in this experiment was $N = 2100$. After the writing exposure was complete, the transmission of the sample was measured by scanning the same laser again over the whole absorption band. To avoid further burning, however, the power of the laser was attenuated by a factor of 10^3. Maximum optical density change of each hole is about $\Delta OD \approx 0.1$. This means that only about 10% of the total number

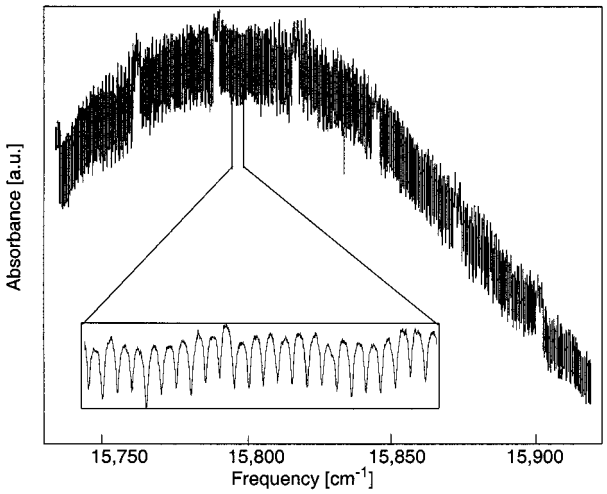

Figure 2. Transmission of an inhomogeneous band after burning a large number of spectral holes with a narrow-band dye laser. Total number of holes is about 2100. Each hole is 0.1 cm^{-1} wide. The sample is a chlorin-doped polymer film at $T = 2$ K.

of molecules was burnt out at each illumination frequency. The inset shows an expanded view of a 75 GHz (0.1 nm) segment of the spectrum. Note that the profiles of each individual hole are clearly resolved. Note also that the width of individual holes, $\Delta\nu_H \approx 800$ MHz, is about two times larger than expected from the homogeneous ZPL width at this temperature. The broadening of the holes in this experiment may be attributed to saturation effects due to a high illumination intensity during writing exposure.

At this point, it is interesting to compare the wavelength resolution of a conventional color photographic film to that of the PSHB material. Whereas a conventional color photograph is composed of three basic colors, a "color" photograph captured by a PSHB material could resolve thousands of wavelengths, each corresponding to a narrow spectral hole. This unique property may be used for hyperspectral imaging of various physical phenomena, including astrophysical objects. Figure 3 shows an experiment in which a dye-doped polymer film, analogous to that described above, was used to capture a highly frequency-resolved picture of the sun.[24] A coeleostatic mount was used to project the image of the sun onto the sample inside a liquid-helium cryostat. The illumination intensity, measured in the plain of the image, was 25 $\mu W/cm^2$ per 1 GHz frequency interval. An average exposure time was about 4 min. The transmission of the sample was measured before and after the exposure by shining a weak expanded beam of a single-mode dye laser through the sample and by capturing the transmitted image with a digital CCD camera. Figure 3a shows one of about 10 000 captured images. Each such image corresponds to one "color" in the total scanning range of the laser, 630−640 nm, and has a resolution of $\Delta\lambda \approx 10^{-3}$ nm. The power of the present method consists of the fact that by a subsequent computer analysis of the recorded images, it is possible to evaluate the sun's emission spectrum at each spatial spot of the sun disk. Figure 3b shows one such spectrum, which was obtained by averaging the signal fern in an area indicated in Figure 3a. The distinct line structure comes from Fraunhofer lines in the emission spectrum of the sun, which is superimposed with some absorption lines in the earth's atmosphere. It is now possible to distinguish between these two to types of lines by simply noting that the position of a Fraunhofer line should experience a Doppler shift due to rotation of the sun, whereas atmospheric lines are constant (Figure 3c). Let us note that an estimated total amount of data, which was collected in the course of this

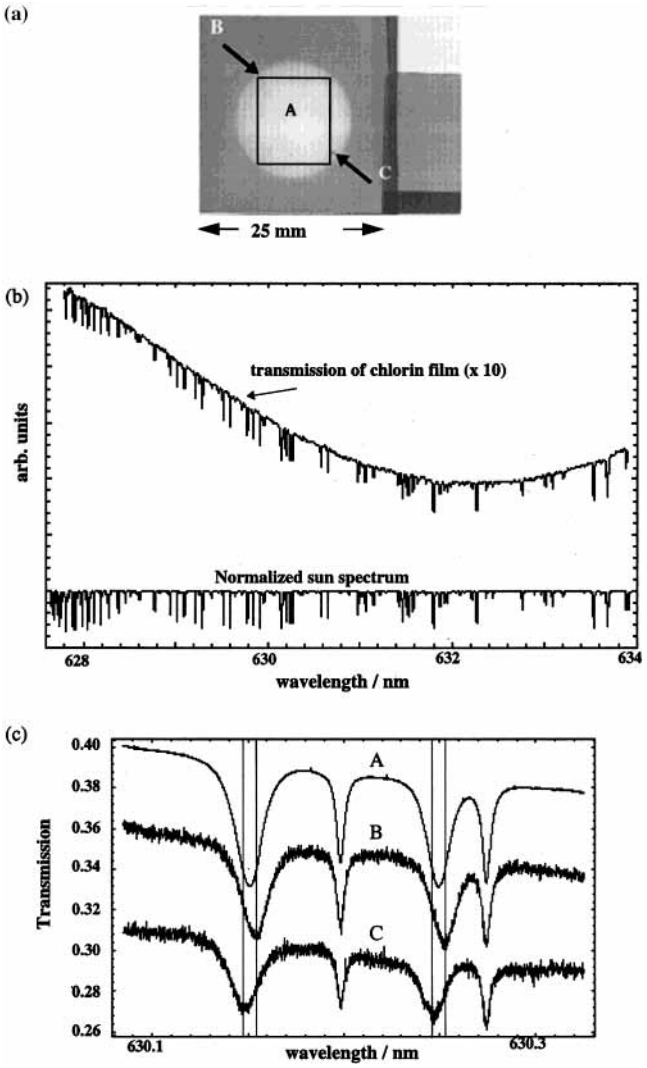

Figure 3. Image of the sun at a single frequency (a). For the read-out of one experiment, more than 10 000 images have to be read out. Panel b shows the spectrum read out from the SHB sample after the exposure. It covers a large part of the usable spectral range of the inhomogeneous band. Panel c shows the spectra extracted from opposite limbs of the solar equator containing solar lines that are mutually Doppler-shifted (because of solar rotation). Note the fixed position of the lines that are caused by the Earth's atmosphere.

experiment, was about 25 GB and that all of these data have been recorded on a single 2 × 2 cm^2 piece of a dye-doped polymer film. The corresponding data transfer rate, at which all of this information was recorded on the PSHB film during the 4-min exposure time, was about 100 MB/s.

2.2. Detection of Spectral Holes in Time Domain. According to basic Fourier theorem, any change made in the frequency-domain transmission of the PSHB medium leads to a corresponding change in the time-domain impulse response of the sample. This kind of direct relation, which often exists in coherent optics between frequency and time coordinates, can be used as an alternative approach for burning and detection of spectral holes.[6,12−16] Two different kinds of experiments on time-domain PSHB have been demonstrated so far. In the first case, both the burning procedure and the detection procedure are performed by using short laser pulses. As will be explained below, this kind of "all time domain" is closely associated with phenomena commonly known as photon echo, more specifically, stimulated photon echo. In the second case, which we may call also a "spectral synthesis" experiment, the holes are actually carved in by a frequency-tuned, narrow-band laser source and only the readout is performed with short pulses in time domain. Below, we will give a brief theoretical introduction to time-domain experiments described later in this paper.

In our experiments, laser pulses have a low or moderate intensity, such that the rate at which molecules are excited is always less than the saturation rate of the transition. Under these conditions, the PSHB medium is acting in a similar manner as a linear spectral filter, and therefore, its time-domain impulse response function may be expressed as

$$K(t) = \frac{1}{2\pi}\int_{-\infty}^{\infty}\tilde{K}(\nu')\, e^{i2\pi\nu' t}\, d\nu' \tag{7}$$

Here, $\tilde{K}(\nu)$ is a complex frequency-domain response function, which is related to the intensity transmission of the sample according to

$$\tilde{K}(\nu) = \sqrt{T(\nu)}\, e^{i\varphi(\nu)} \tag{8}$$

where $\varphi(\nu)$ is the phase shift associated with dispersion. Whereas the intensity transmission function, $T(\nu)$, is often readily available from the experiment by performing a direct measurement of the spectrum, the associated phase function cannot be easily obtained. This apparent difficulty may be overcome, however, by noticing that for a passive absorbing filter like a PSHB medium, the phase is given by the so-called minimum phase condition (also called the Hilbert phase):[25]

$$\varphi(\nu) = \frac{1}{\pi}P\int_{-\infty}^{\infty}\frac{\ln\sqrt{T(\nu')}}{\nu - \nu'}\, d\nu' \tag{9}$$

where P in front of the integral means principal value, and the whole expression represents Hilbert transformation. The last relation is well-suited for numerical evaluation of the phase in case of an arbitrary transmission, $T(\nu)$, including for spatially heterogeneous samples and for samples with large optical density. Sometimes, however, it is still an advantage to have a simple analytical expression for the phase. A particularly physically transparent situation arises in connection with absorption coefficient, described by eq 6, where the hole profile is Lorentzian and is invariant through the thickness of the sample. In this case, the absorption coefficient and index of refraction are given, correspondingly, by the imaginary and the real part of the complex Lorentzian:

$$\tilde{\gamma}(\nu) = \frac{2\Gamma_{ZPL}}{(\nu_0 - \nu) - i2\Gamma_{ZPL}} \tag{10}$$

The phase change is then given by

$$\varphi(\nu) = \frac{2\pi\nu d}{c'}\Delta n(\nu) \tag{11}$$

where c' is the velocity of light in the medium and the refractive index change, $\Delta n(\nu)$, is given by convolution of the hole profile with the dispersive part of the Lorentzian:

$$\Delta n(\nu) \propto \int_{-\infty}^{\infty} I_L(\nu')\, \mathrm{Re}\, \tilde{\gamma}(\nu - \nu')\, d\nu' \tag{12}$$

Note that for a weakly absorbing medium, such as used in our experiment, the minimum phase condition given by eq 9 becomes essentially equivalent to Kramers−Kronig dispersion relations between the absorption coefficient and the index of refraction.

Formulas 1−12 allow calculation of the coherent optical response of a PSHB medium containing any arbitrary spatial-spectral hole profile. As an example, let us consider that a PSHB plate contains a single narrow spectral hole, which is centered at frequency, ν_1. Let us assume that the sample is illuminated with a short bandwidth-limited probe pulse of amplitude, $E^{\text{in}}(t)$. At the output of the sample, the transmitted pulse amplitude will be

$$E^{\text{out}}(t) = \frac{1}{2\pi}\int_0^\infty E^{\text{in}}(\nu')K(\nu')\, e^{i2\pi\nu' t}\, d\nu' \qquad (13)$$

where the frequency-domain amplitude is related to the time-domain amplitude by Fourier transform:

$$E^{\text{in}}(\nu) = \int_{-\infty}^{\infty} E^{\text{in}}(t')\, e^{-i2\pi\nu t'}\, dt' \qquad (14)$$

Because frequency ν_1 is transmitted more than all other frequencies, the power spectrum of the output pulse will be, in effect, narrower than the spectrum of the input pulse. Accordingly, the temporal profile of the pulse will be also stretched out in time. By measuring the change of the shape of the pulse as it passes through the sample, we obtain an equivalent amount of information, as by measuring the spectral profile of the hole in frequency domain.

In an actual experiment, it is often easier to measure the time response of not just one spectral hole but a set of multiple holes separated in frequency by a constant interval. Such a frequency "comb" is created, for example, if hole burning is performed with a periodic train of pulses. Figure 4 shows an experiment[6] in which the PSHB material was illuminated with a train of picosecond pulses with an interval of $\Delta t = 80$ ps. The pulses had an overall spectral width of $\Delta\nu_{\text{L}} = 150$ GHz. After the burning exposure, the spectral transmission was measured by a scanning narrow-band laser. The period of the hole pattern, $\Delta\nu = 0.42$ cm^{-1}, was equal, as expected, to the inverse value of the time delay. Figure 4b shows the result of probing the periodic hole structure with a picosecond pulse. The transmitted pulse shape comprised a series of pulses, which were delayed by time intervals Δt, $2\Delta t$, $3\Delta t$, etc. The pulse at zero delay may be identified with the directly transmitted laser pulse, while the pulses at 80 ps and 160 ps are the time-domain manifestation of the spectral holes.

2.3. Spectral Holes in External Electric Field. Molecules that have a static electric moment are often used in spectroscopy as sensitive probes of electric field. If placed in an external field, the transition frequency of such molecules may experience a shift due to Stark effect. In the kind of organic dye molecules studied in this paper, the dominant contribution to the shift comes from linear Stark effect:

$$\Delta\nu_{\text{Stark}} \propto (\vec{E}\cdot\Delta\vec{\mu}) \qquad (15)$$

where $\vec{E}$ is the electric field strength and $\Delta\vec{\mu}$ is difference between the electric dipole in the ground and excited states. Note that the inhomogeneous line broadening itself may be considered as resulting from random frequency shifts induced by different local electric fields. We can estimate the magnitude of $\Delta\nu_{\text{Stark}}$ if we note that a typical value for dipole moment difference in dye molecules in a solid is about 1 D. In laboratory conditions, maximum applied electric field strength is about 10^7 V m^{-1}. Accordingly, the largest Stark shift that we can expect to obtain in our experiments is on the order of 10 GHz. This value is more than 10 times the value of Γ_{ZPL} at low temperature but is still several orders of magnitude less than inhomogeneous broadening. As we will show below, this combination of molecular parameters turns out to be well-suited for manipulating spectral holes and holograms with externally applied electric field.

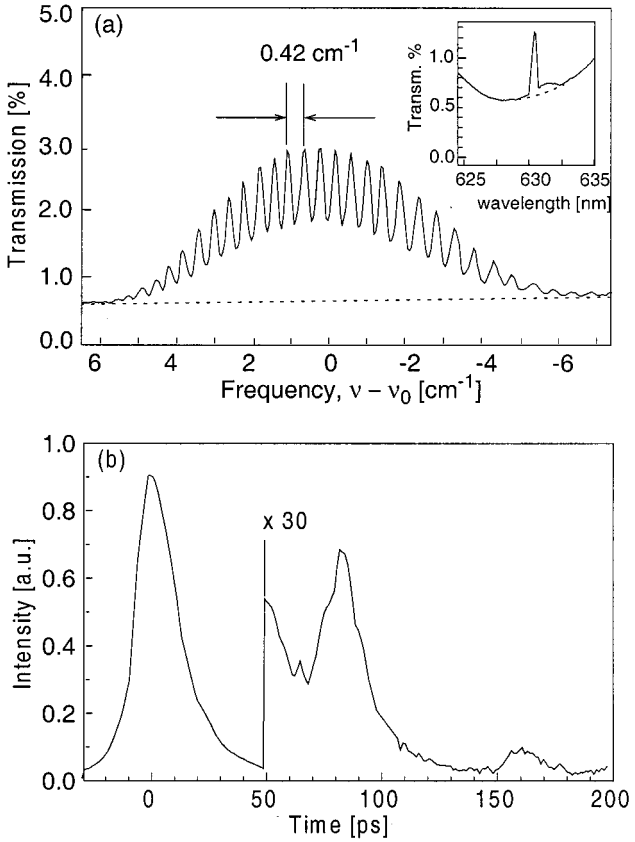

Figure 4. Time-domain detection of spectral holes with picosecond pulses: (a) transmission spectrum of the sample with a "comb" of periodic spectral holes. The dashed line is the transmission before the hole burning exposure; the insert shows the low-resolution envelope shape of the hole. The zero-phonon hole and pseudophonon sideband are visible. Panel b shows the time-domain transmission of the sample measured with a picosecond streak camera. Pulses at 80 and 160 ps correspond to the coherent response of the holes; the pulse at zero time is the transmitted laser pulse.

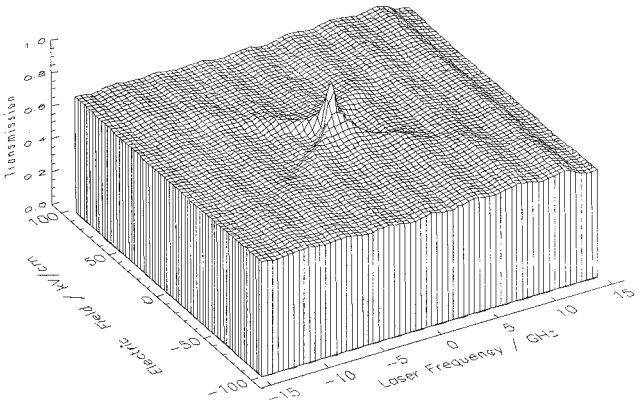

Figure 5. Spectral transmission of a single spectral hole measured at different values of applied external electric field.

Figure 5 shows the transmission of a narrow hole at different values of $\vec{E}$.[26] The hole was burnt in the center of the inhomogeneous band at $\vec{E} = 0$. When the field was applied, the hole profile broadened and eventually split into two components, which then gradually faded out as the field strength was increased further. When the field was turned off again, the initial hole shape was immediately restored. On a qualitative

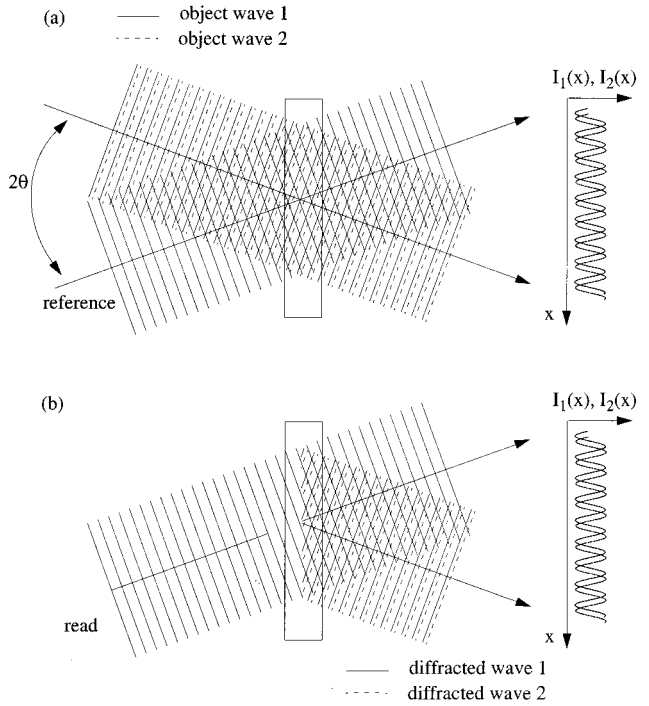

Figure 6. Principle of holographic recording (a) and read out (b). The recording of a second hologram with slightly shifted phase shows how the phase of the object wave is transferred to the hologram and, subsequently, to the diffracted light wave.

level, this behavior may be easily understood, if we consider that, prior to the burning, the inhomogeneous band consists of molecules with all possible orientations in space. Therefore, in an unburned sample, the Stark shifts are random and do not change the absorption profile, because for every number of molecule shifting to the higher frequency, there is a statistically balanced number of molecules shifting in the opposite direction. Illumination with a linearly polarized monochromatic light disturbs this balance by bleaching out preferentially those molecules that have their optical transition dipole moment, $\vec{d}$, oriented parallel to the optical polarization vector, $\vec{n}$. On the other hand, the relative orientation of $\vec{d}$ and $\Delta\vec{\mu}$ is determined by the molecule's structure. Therefore, PSHB creates also a deficiency of molecules with certain orientations of $\Delta\vec{\mu}$, and as external field is applied, the shape of the hole starts to deform. A detailed quantitative analysis of hole shape as a function of electric field may be found in ref 27, which also describes various spectroscopic applications of this effect. In this paper, we utilize Stark effect mainly to manipulate properties of diffraction gratings to perform optical calculation and signal processing.

3. Frequency Domain Holography

An elegant way to perform a PSHB experiment is to create a spatial grating pattern by using interference between two monochromatic waves.[10] Figure 6a shows two linearly polarized monochromatic light waves of frequency ν_0 and with intensities I_1 and I_2, propagating in the $x-z$ plane and crossing at an angle of 2θ. Normalized spatial-spectral intensity, measured in the $x-y$ plane is

$$I_L(\nu,x,y) = [1 + V\cos(2\pi(x/\Lambda) + \phi)]\delta(\nu - \nu_0) \quad (16)$$

where $\Lambda = c/(2\nu_0 \sin\theta)$ is the spatial period of the fringes and $V = (2\sqrt{I_1 I_2})/(I_1 + I_2)$ is the fringe visibility function. Phase ϕ describes the shift of fringe maxima with respect to the origin of the x-axis. Note that, in principle, all of the three parameters, Λ, V, and ϕ, may vary as a function of frequency. For now, we will assume that all of these parameters are constant and leave a more general discussion for later. Because the illumination intensity varies periodically with the x-coordinate, the depth of the burnt hole will also vary accordingly in space with the period Λ. We can say that the interference pattern is "imprinted" into the PSHB medium, giving rise to diffraction grating in space and in frequency dimension.

If the sample is illuminated with a monochromatic read beam, then such periodic grating will give rise to diffracted waves, as is shown in Figure 6b. However, unlike conventional gratings, the diffraction will be present only in the narrow interval of frequency in the region of the spectral hole. Therefore, by measuring the diffraction intensity as a function of frequency, one can effectively eliminate background and improve the detection of shallow holes by several orders of magnitude.[10] Even more important is that by this technique one can record and read out in the same sample many holographic images with no or very little cross-talk between different holograms. This is in a sharp contrast to recording of multiple holograms by conventional spatial gratings, which always degrade as the number of holograms increases.

3.1. Diffraction from a Simple Spatial-Spectral Grating. Our next task is to evaluate the diffraction amplitude from a simple spatial-spectral grating. Provided that the thickness of the hologram is much less than the spacing between the fringes in the x direction, $d < \Lambda$, the amplitude of the transmitted monochromatic wave immediately after the plate can be found using the frequency-domain coherent response function defined by eq 8:

$$E^{out}(\nu,x,y) = E^{in}(\nu)\tilde{K}(\nu,x,y) \quad (17)$$

Here, we are considering the simplest case, where the grating has a low contrast and the contribution of the phonon sideband to the absorption is neglected. Then the frequency domain coherent response may be reduced to

$$\tilde{K}(\nu,x) \propto \int_{-\infty}^{\infty} I_L(\nu',x)\tilde{\gamma}(\nu' - \nu)\, d\nu' \quad (18)$$

By substituting eq 16 into eq 18, we find that the output amplitude consists of two amplitudes diffracted in complementary directions and a nondiffracted (but attenuated) read wave. The diffracted amplitude propagating closest to the positive x-axis direction may be expressed as a sum of two terms:

$$E_{dif}(\nu) = E_\alpha(\nu) + iE_n(\nu) \quad (19)$$

where

$$E_\alpha(\nu) = \mathrm{Im}\,\tilde{\gamma}(\nu) = \frac{2\Gamma_{ZPL}}{(\nu_0 - \nu)^2 + (2\Gamma_{ZPL})^2}$$

$$E_n(\nu) = \mathrm{Re}\,\tilde{\gamma}(\nu) = \frac{(\nu_0 - \nu)}{(\nu_0 - \nu)^2 + (2\Gamma_{ZPL})^2} \quad (20)$$

This relation shows that diffraction from a spatial-spectral SHB structure has a contribution from both absorption index grating and the refraction index grating. It is a most remarkable property of PSHB that it allows changing the absorption coefficient and, correlated to it by Kramers−Kronig dispersion relations, the index of refraction with a high precision in the frequency dimension, as well as in space. Note that amplitudes

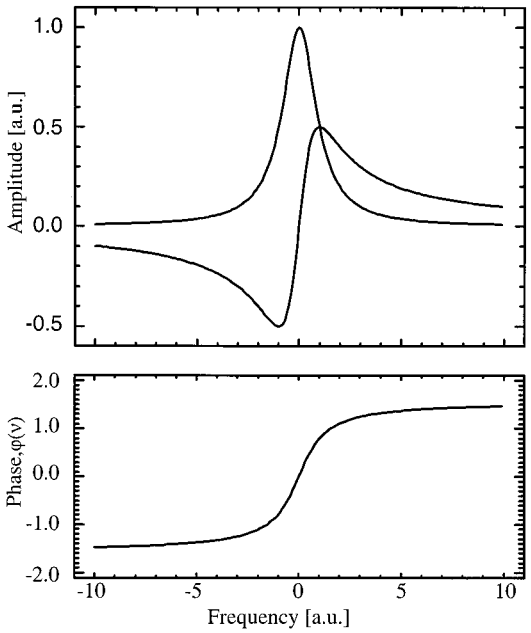

Figure 7. Light amplitude diffracted from the absorption grating and the refractive index grating (a), associated with a single narrow spectral hole and (b) frequency dependence of the phase of combined diffracted amplitude from both gratings.

scattered by refractive grating and absorption grating are shifted in phase with respect to each other by $\pi/2$. The total diffracted intensity is given by superposition of the two contributions.

Figure 7 shows the amplitudes diffracted from the absorptive and refractive grating as a function of frequency. Note that the sign of the refraction index part changes to the opposite in the vicinity of exact resonance. Also, the refractive part falls off much slower with frequency than the corresponding absorption part. For this reason, a certain amount of diffraction may be detected even if the frequency offset is as large as several line widths. This peculiarity determines interaction and cross-talk between holograms, especially if many holograms are recorded at adjacent frequencies.

If the sample is geometrically thick, such that $d \geq \Lambda$, then the output of the hologram will depend on wave matching conditions similar to that of conventional thick volume holograms. In particular, Figure 6 shows only one diffracted wave because the conjugated wave is strongly attenuated by the wave matching condition. In that case, the hologram's diffraction efficiency may be calculated using a modified Kogelnik's coupled wave theory.

3.2. Frequency and Phase Swept Spatial-Spectral Gratings. Let us now consider two gratings at frequencies ν_1 and ν_2. If the separation between the frequencies is much larger than the homogeneous line width, $(\nu_2 - \nu_1) \ll \Gamma_{hom}$, then each grating will diffract in a different frequency. However, if the frequency separation becomes comparable to the line width, then the diffracted amplitudes will start to interfere with each other. Because the spatial phases of the two gratings, ϕ_1 and ϕ_2, are not necessarily the same (in fact, the phase of each grating may be arbitrary), a rather involved behavior of destructive and constructive interferences, which occur between absorption and refraction parts of different gratings, arises. These interferences were first studied in ref 28, and also in ref 29, in which the dimension of an external electric field was added to the picture. It was noticed that if many holograms were recorded at adjacent frequencies, then the interference had an accumulating effect, especially because of the far-reaching "tail" of the index of refraction. Such accumulated interference reduced the efficiency of the hologram readout. It also significantly impaired our ability to store a large number of holograms in the frequency dimension. In the studies described below, we have investigated in detail the cause of such interference and have found ways to overcome these negative effects.

The key to solution of the problem consists of controlling the relative phase, $\Delta\phi = \phi_2 - \phi_1$, between the gratings. This idea was first introduced when we found that diffraction from a thin grating, which is normally symmetrical in positive and negative scattering directions, becomes asymmetrical if two adjacent gratings are recorded with a certain frequency-dependent phase shift.[30] By sweeping the frequency of the burning laser over a range of a few homogeneous line widths and by varying the phase between the writing object and reference beams as a linear function of frequency, $\Delta\phi = \text{Const}\cdot\nu$, we observed that the efficiency of diffraction in one scattering direction increased, while signal diffracted in the conjugated direction practically vanished. What is even more important, the undesired interaction between gratings in the amplified diffraction direction was reduced by controlling the phase. The physical reason, which is connecting the asymmetry of diffraction with the reduced cross-talk, consists of the principle of causality and is discussed in refs 12 and 30. Here we are interested in using this approach for optimizing the diffraction properties of PSHB holograms. Gratings, which are written by manipulating the frequency-dependent amplitude and phase, are called in the literature frequency and phase swept (FPS) gratings.

A FPS grating is typically described by two functions—amplitude profile, $A(\nu)$, and phase profile, $\phi(\nu)$. The amplitude profile can be implemented by modulating the intensity of the writing beams as the frequency of the writing laser is changed. Correspondingly, the phase profile may be implemented by modulating the retardation between the object and reference beams. As a result, the PSHB medium will contain a complicated continuously varying spatial-spectral grating, which may be different at every frequency. Note that, because amplitude and phase functions may be chosen independently, one may create, in principle, a great variety of different FPS gratings.[31,32]

Formula 8 gives a quantitative description of diffraction from any arbitrary spatial-spectral structure, including FPS gratings, if the corresponding spatial-spectral transmission function, $T(\nu,x)$, is known. For a simplified qualitative description, it is better to use expressions similar to eqs 19 and 20. In this approach, the amplitude diffracted by a FPS grating may be expressed as

$$E'_{FPS}(\nu) = \int_{-\infty}^{\infty} E_{diff}(\nu')\tilde{S}(\nu' - \nu)\, d\nu' \qquad (21)$$

where $E_{diff}(\nu)$ is amplitude-scattered by a simple one-frequency grating and $\tilde{S}(\nu)$ is a so-called complex "sweep" function,

$$\tilde{S}(\nu) = A(\nu)\, e^{i\phi(\nu)} \qquad (22)$$

It turns out that by choosing special $A(\nu)$ and $\phi(\nu)$, it is possible to improve the diffraction efficiency, to reduce the crosstalk between spectrally adjacent holograms, and to improve the stability of the holograms against bleaching during read, which all amounts to controlling the diffraction in various important ways. Figure 8 shows spectral intensity profiles of different FPS gratings. The integrated exposure used to write each hologram was held constant. The single-frequency hologram (I) represents a trivial case with no FPS. Here, the holographic grating was written while the laser was parked at one frequency, that is, $A(\nu)$ is essentially a δ-function and the

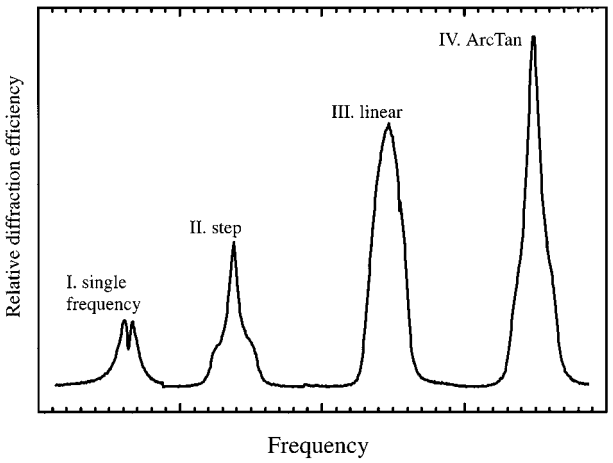

Figure 8. Relative diffraction efficiency of various types of FPS gratings (see text).

associated phase is a constant. The diffraction efficiency of such a straightforward grating never exceeded 0.5%, independent of the writing exposure. Furthermore, holograms recorded without using the FPS technique are subject to saturation, which is manifested as a pronounced dip at the center of the spectral profile. As we have mentioned before, for high-density storage, such simple holograms are of limited utility because of strong cross-talk between adjacent frequencies. In three other holograms, the writing laser is scanned uniformly over a frequency interval of about 1 GHz, while the phase is modulated in various fashions. This frequency scan corresponds to an amplitude function in the form of a rectangle such that inside the burning interval $A(\nu) = 1$ and outside of this interval $A(\nu) = 0$.

In case II, the phase is also kept constant, with an exception of an abrupt phase jump of π at the center frequency. The type, which we call a π-jump hologram, may be viewed as consisting of two spectrally adjacent partial holograms, each of them recorded over a few line widths. The purpose of the π phase shift is to achieve constructive interference of the refractive index contributions at frequencies between the two partial holograms and especially at the center frequency. At frequencies outside the burning interval, the refractive indexes interfere destructively. At the same time, the absorption contributions interfere destructively at all frequencies, including at the center frequency. The destructive interference at outside frequencies suppresses cross-talk between adjacent gratings. The diffraction efficiency peaks at the center of the hologram and has there a higher value than the non-FPS hologram. What is more important, however, is that such a "pure" refractive index hologram turns out to be very robust against bleaching during the read-out (see below). In case III, which we call linear FPS, the phase of the grating is altered as a linear function of frequency such that the total phase shift between minimum and maximum frequencies amounts to 2π. Such holograms have a markedly higher diffraction efficiency and practically no cross-talk. Let us note that a linear phase shift may be implemented by introducing a suitable optical path length difference between the interfering beams. Like in pulsed SHB experiments described below, this leads to an amplification or suppression of particular diffraction orders, depending on the sign of the delay. Finally, in case IV, the phase is changed according to an arctan function, which appeared previously in Figure 7. The idea behind the arctan sweep function is to bring both contributions, from absorption as well as from refraction, to a constructive interference at the center frequency. This results in the peak diffraction efficiency as high as 4.8%.[31]

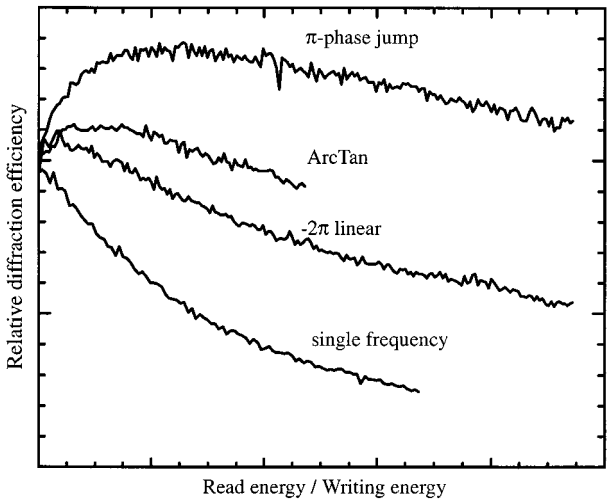

Figure 9. Comparison of bleaching behavior of the different FPS gratings as a function of relative readout energy.

Figure 9 displays another special aspect of FPS holograms, which consists of improved endurance with respect to a degradation caused by illumination during read-out. A set of holograms were written in with equal burning energy in a frequency interval of six holewidths. After the writing exposure, the holograms were read out at their center frequency with the same intensity, and the change of the absolute diffraction efficiency was measured as a function of the read out time. For a direct comparison, the time axis is presented in units of the time interval used for writing. The plot shows that a trivial single-frequency hologram degrades rapidly and its diffraction efficiency drops to about 20% of the initial value when it is illuminated with the same total amount of energy as that used for writing. In contrast, various FPS holograms degrade much more slowly and in some cases even show at first an increase or amplification. Such markedly improved endurance may be explained if we consider that by illuminating a FPS grating at the center frequency, we are decreasing loss due to absorption while retaining the refractive index part of the grating. This latter part is formed mainly by molecules at the wings of the burning range. Note that the refractive index contribution is most dominant for the π-jump grating and as expected, this type of hologram provides the best read-out stability of all examples shown here.

3.3. Image Holograms and Holographic Movie. One of the main applications of the recording techniques described above consists of storage and reproduction of multiple image holograms. By rapidly reading out a series of holographic images, one can create an impression of a three-dimensional movie. Figure 10 shows a setup used in our image storage experiments. The output of a frequency-tunable single-mode dye laser (Coherent CR 899-29) with a line width of $\sim$1 MHz is split into reference and object beams, which then overlap at a SHB sample inside a helium bath cryostat. The object beam comprises either an interchangeable slide mask or a liquid crystal spatial light modulator. The object image was focused on a 16-bit CCD camera (Astromed CCD 2200). The relative phase between the object and the reference beams was controlled by a mirror mounted on a piezo-electric transducer and was monitored by detecting the position of spatial interference fringes with a photodiode array detector. To write an image hologram, the sample was illuminated simultaneously with reference and object beams. Reconstruction was accomplished by illuminating the sample with the reference beam only. The SHB sample consists again of chlorin-doped polyvinylbutyral film at a temperature

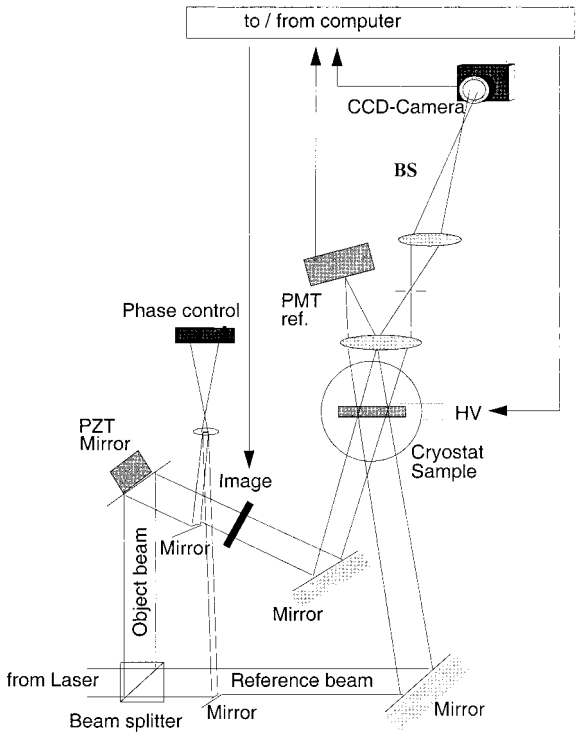

Figure 10. Experimental setup used for holographic image storage. Abbreviations are as follows: BS = beam splitter; PMT = photomultiplier; HV = high voltage.

of 1.7 K. The sample was pressed between glass plates covered with semitransparent electrodes.

Figure 11 shows 25 image holograms recorded by using five different burning frequencies and five different values of applied voltage.[33] At each laser frequency, five different images were stored by changing the applied field strength in the range ± 150 kV cm^{-1}. Writing of each hologram required an irradiance of 50 μW cm^{-2} and an exposure time of 5 s. The overall spectral bandwidth utilized in this experiment was only 1 cm^{-1} (30 GHz), which is only small fraction of the overall inhomogeneous bandwidth available in this material. In the next experiment, the laser was scanned over the whole inhomogeneous band, which allowed storage of a much larger number of holograms. Figure 12a shows selected images from a series of 2100 stored holograms.[8] For writing the holograms, individual frames of an 80 s segment of an animated cartoon were displayed on an 8-bit 350 $\times$ 280 pixel LCD positioned in the object beam. Here, we used the FPS technique described above, consisting of a linear 2π phase change per 1 GHz interval. Electric field multiplexing provided the storage of seven cartoon frames plus one blank image at every spectral hole location. The holograms were read out by parking the laser frequency in the center of the FPS region and by setting the appropriate electric field value. This experiment demonstrated that a large number of quality image holograms may be recorded by PSHB in a single sample without cross-talk. Figure 12b shows a slightly different experiment in which the object was a true 3-D toy bunny. Multiple views were recorded by rotating the bunny. Sequential read out created a complete impression of a rotating 3-D object.

We have further investigated quantitative limits to the storage capacity of this material and have shown that 6000 image holograms can be recorded using frequency and electric field multiplexing.[34] Finally, we have recorded 12 000 images using the whole absorption band, thus reaching the ultimate theoretical limit defined by the ratio of the inhomogeneous and homogeneous line width.[35] It is interesting to note that in the last

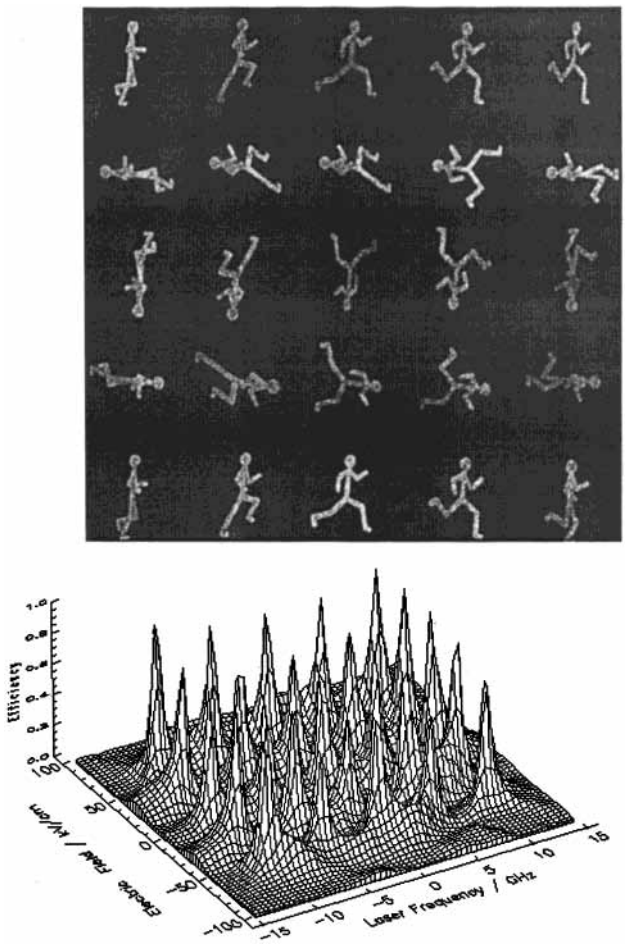

Figure 11. Storage of 25 images (stickmen) in a plane given by wavelength and electric field. To avoid cross-talk, a phase shift of π was applied with respect to nearest neighbors.

experiment the estimated average number of dye molecules per 1 μm^2 of every hologram is as small as 500. At the same time, the average number of photons diffracted from this area in one second is about 10^2-10^3, corresponding to an absolute diffraction efficiency on the order of 10^{-5}. The calculation yields a result of 60−600 photons per second in a spot of 1 μm^2 in size. Our data shows that we have actually approached the limit minimum number of 100 photons per bit, which is needed for reliable detection.

Let us also note that in our experiments the image resolution is limited by the properties of LCD and other optical components rather than by the spatial resolution of the PSHB material. For our current optical system, we estimate that the upper limit for the storage density is 10^{10} bit/cm^2. With an area density of the dye molecules of about 3×10^{16} cm^{-2} and provided that high-quality diffraction-limited optics would be used, we estimate that an area storage density of more than 10^{12} bit/cm^2 is possible. A further consideration of the data storage capacity should include bit error rate and error-reduction algorithms.

3.4. Frequency-Domain Processing by Stark Effect. Conventional optical processing is founded on interference and other coherent properties of monochromatic light. A PSHB-based optical processor makes, in addition, use of spectroscopic properties of molecules, especially of the behavior of energy levels in an external electric field.[36] As we have shown before, holograms with specific relative phase may be recorded at different frequencies. Spectral overlap and therefore interference between the holograms may be switched on and off by applying

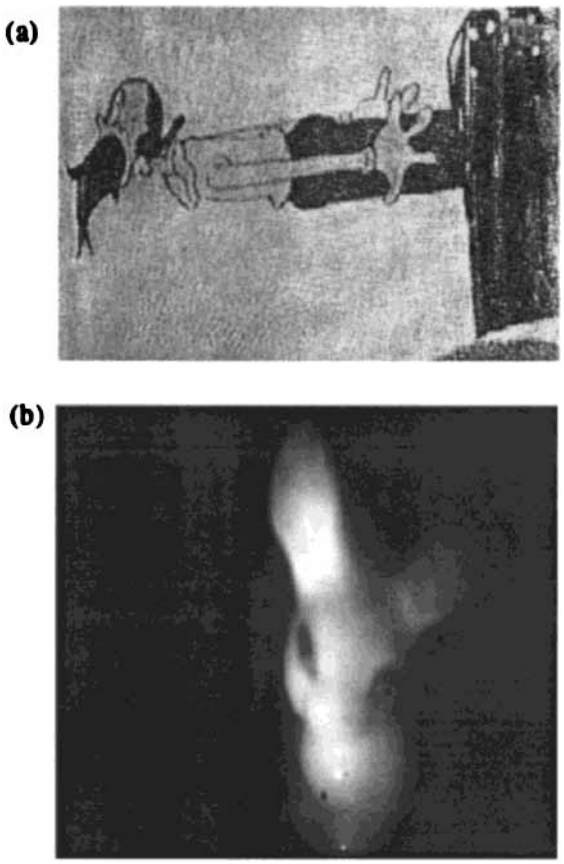

Figure 12. Images used in the holographic image storage experiments: (a) Popeye; (b) bunny, used for the real time holographic movie.

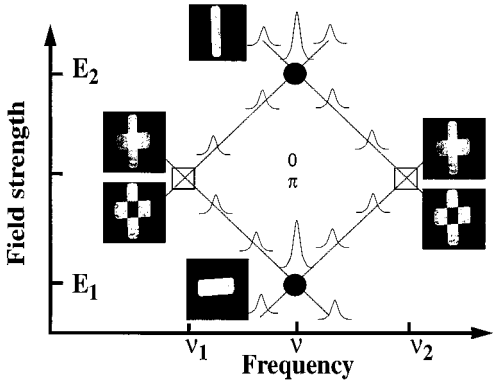

Figure 13. Illustration of the interference regions (squares) of holograms recorded in the frequency−electric field plane. Different holograms were recorded in the electric field dimension. Recording positions are indicated by black circles.

an external electric field. In this sense, the molecular system itself acts as a parallel information processor—a molecular computer.

Figure 13 shows how logical operations may be performed by switching the electric field strength in a "molecular computer". The system consists of two PSHB holograms, burned in at the same laser frequency, ν, but at different electric field strengths, E_1 and E_2. At an intermediate electric field value, $E \approx (E_1 + E_2)/2$, the frequency profiles of both holograms are split into two peaks, each shifted by $\pm\Delta\nu$. If the frequency of the read out laser is tuned to $\nu + (-) \Delta\nu$, then one can observe interference between the two holograms. Depending on the relative phase, either constructive or destructive interference may

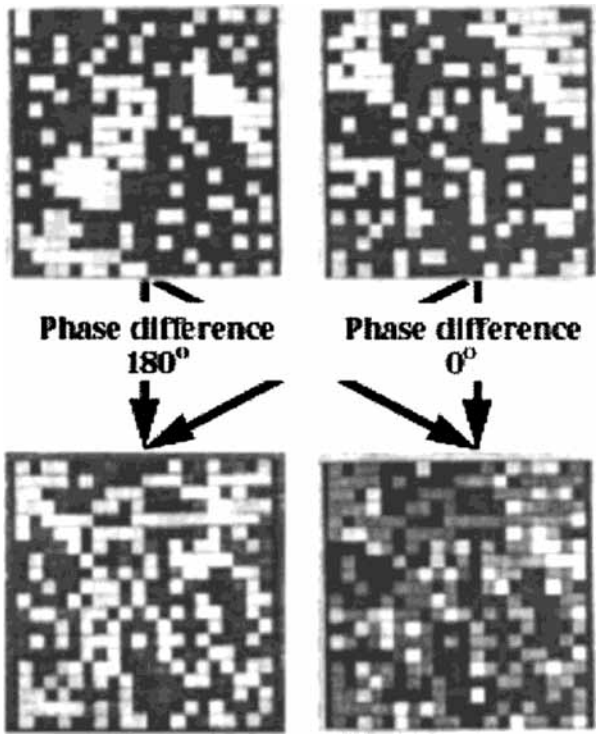

Figure 14. Two input patterns recorded at equal frequencies and adjacent electric fields. In the lower row, the superposition of the images with different phase shifts is shown. By appropriate discrimination, the logical operations AND and XOR can be obtained from the interfering images.

be obtained. As a further development based on the same switching principle, Figure 14 shows a coherent superposition of two different 20 × 20 binary image patterns. If at a given spatial location both holograms have a bright pixel, and if the phase difference between the holograms is an integer number of 2π, then one observes constructive interference and a bright pixel. If the phase difference is 180°, then destructive interference results in a dark pixel. By discriminating between bright and dark pixels, it is possible to implement logical operations such as "AND", "OR" (from constructive interference), and "XOR" (from destructive interference).

Another potential application of PSHB consists of implementing neural networks and error-corrective memories. The possibility of addressing data in frequency dimension is again an important advantage over conventional techniques because it allows multiple independent interconnects using the same spatial channel.

4. Time Domain Holography

The term "time domain holography" refers to recording of optical amplitudes that vary in time. A remarkable property of PSHB medium consists of its ability to record and play back such time-domain signals. As we discussed above, for a geometrically thin medium, linear coherent optical responses in frequency domain and in time domain are related to each other by Fourier transformation, and both functions may be calculated from known spatial-spectral intensity transmission of the medium, $T(\nu,x,y)$. One purpose of this paper is elucidating the connection between the time- and frequency-domain versions of PSHB holography and showing that, in fact, these can (and should) be viewed as complimentary manifestations of the same phenomena, inherent to inhomogeneously broadened systems.

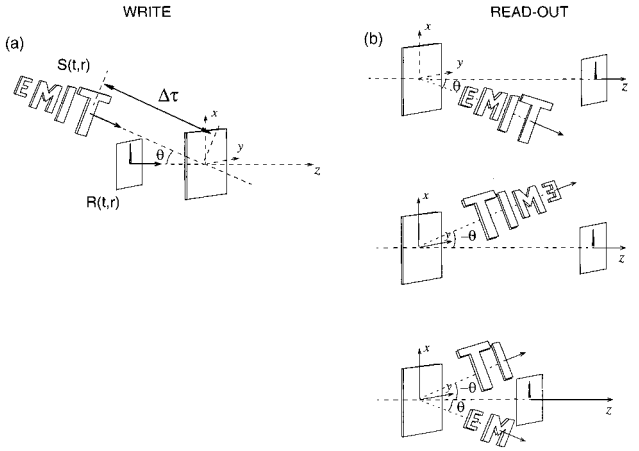

Figure 15. Scheme of recording (a) and play-back (b) of time-and-space-domain holograms (see text for explanations).

In time-domain storage, the information occurs as a continuous chain of scenes or events. Instead of writing a separate holograms for every scene, a whole set of holograms at different frequencies is written in at once and in parallel. Also, during the read out, different holograms are played back in one single coherent laser flash. This is possible because the PSHB hologram contains information about both the amplitudes and the relative phases of the spectral components of the signal. As we will now show, a time-and-space-domain hologram recalls both the spatial structure and the complete temporal shape of the object amplitude.

Maximum duration, Δt_{max}, of the recorded time-and-space-domain scene is fundamentally limited by optical coherence time (also called optical dephasing time), T_2. The value of T_2 is given by the inverse of the homogeneous ZPL line width, $T_2 = (\pi\Gamma_{ZPL})^{-1}$. In the organic systems used in our experiments, $T_2 \approx 1$ ns. On the other hand, the inhomogeneous bandwidth defines the shortest duration of an event that can be recorded, $\Delta t_{min} \approx \Gamma_{inh}^{-1}$. This allows us to make full use of the fact that in dye-doped polymers the inhomogeneous width is as large as 5−10 THz, and apply it for recording and play-back of optical signals with an unprecedented femtosecond resolution in time domain.

4.1. Recording and Playback of Time-Domain Holograms. Figure 15a shows one possible arrangement for recording of time-domain holograms. Following refs 12 and 37, consider that a geometrically thin plate of PSHB material is illuminated with an object beam of time-space amplitude

$$S(t,\vec{r}) = s\left(t - \frac{\vec{n}_s \cdot \vec{r}}{c} - \Delta\tau, x, y\right) e^{i2\pi\nu_0(t-(\vec{n}_s\cdot\vec{r}/c)-\Delta\tau)} \quad (23)$$

where $\vec{n}_s$ is unit vector in the direction of propagation of the object pulse and with a plane wave reference beam of amplitude propagating in the *z*-axis direction

$$R(t,\vec{r}) = R_0\delta\left(t - \frac{z}{c}\right) e^{i2\pi\nu_0(t-(z/c))} \quad (24)$$

The object amplitude may have an arbitrary structure both in time and in space, whereas the reference is assumed to be a short δ-like pulse. Propagation directions of the two beams are divided by an angle, θ, and also their arrival times at the plate are divided by time delay, $\Delta\tau$. As in conventional holography, the role of the angle is to allow separation of the diffracted light from the directly transmitted read beam at the output of the hologram. The role of the time delay, however, is unique and is due to the principle of causality, as will be explained below.

The illumination alters the spatial-spectral absorption (and associated refraction) of the medium in proportion to absorbed power. The incident power density in the $x-y$ plane may be found, if we present the object and reference amplitude by their corresponding frequency Fourier components:

$$R(\nu,x,y) = \int_{-\infty}^{\infty} R(t)\, e^{i2\pi\nu t}\, dt$$

$$S(\nu,x,y) = e^{i2\pi\nu((\theta x/c)-\Delta\tau)} \int_{-\infty}^{\infty} s(t,x,y)\, e^{i2\pi\nu t}\, dt \quad (25)$$

Then, the spatial-spectral intensity incident on the PSHB plate is given by

$$I_L(\nu,x,y) = |R(\nu,x,y) + S(\nu,x,y)|^2$$

$$= (R_0^2 + |s(\nu,x,y)|^2) + R_0^* s(\nu,x,y)\, e^{i2\pi\nu((\theta x/c)-\Delta\tau)} + R_0 s^*(\nu,x,y)\, e^{-i2\pi\nu((\theta x/c)-\Delta\tau)} \quad (26)$$

If the combined duration of the object pulse and the delay, $\Delta\tau$, is much less than dephasing time T_2 and if the spectral width of the incident spectrum (eq 24) is much narrower than the inhomogeneous band, then the change of the transmission will be directly proportional to eq 26. In the approximation that we used earlier, the coherent frequency response of the hologram may be found by substituting eq 26 into eq 18. Further, we evaluate the time response of the hologram. For this, we illuminate the PSHB plate with a plain wave δ-like short pulse, identical to eq 25, as depicted in the right-hand side of Figure 15. Equation 13 gives the amplitude at the output of the plate as a convolution of three pulse amplitudes. Again, we find that the scattering amplitude comprises three components, one of which corresponds to transmitted probe wave, which will be neglected. The other two terms can be written as

$$E^{out}(t,x,y) \propto 2\Theta(t)s\left(t + \frac{\theta x}{c} - \Delta\tau, x, y\right) e^{i2\pi\nu_0(t+(\theta x/c)-\Delta\tau)} + 2\Theta(t)s^*\left(-t + \frac{\theta x}{c} - \Delta\tau, x, y\right) e^{i2\pi\nu_0(t-(\theta x/c)+t_s)} \quad (27)$$

where causality is preserved by the Heavyside step function

$$\Theta(t) = \begin{cases} 0 \text{ if } t < 0 \\ 1 \text{ if } t > 0 \end{cases} \quad (28)$$

Notice that because of causality these two terms cannot be both present in full simultaneously. Figure 15b shows how the output of the hologram depends on the relative temporal ordering of object and reference pulses during the recording. Three different cases are considered. If the reference pulse precedes the object pulse, then the hologram plays back a replica of the object including its temporal structure. However, if the temporal ordering of the writing pulses is reversed, that is, if the object pulse is applied before the reference pulse, then the hologram plays back the conjugated wave front of a time-inverted replica of the object. In the intermediate case, if the reference arrives simultaneously with the object pulse, the recalled signal is split into two parts, which are propagating in conjugate directions. The earlier part is recalled as a conjugated time-inverted replica, whereas the later part is reproduced as a noninverted replica.

This peculiar dependence of diffraction on delay occurs because causality serves as an intrinsic "time arrow", which

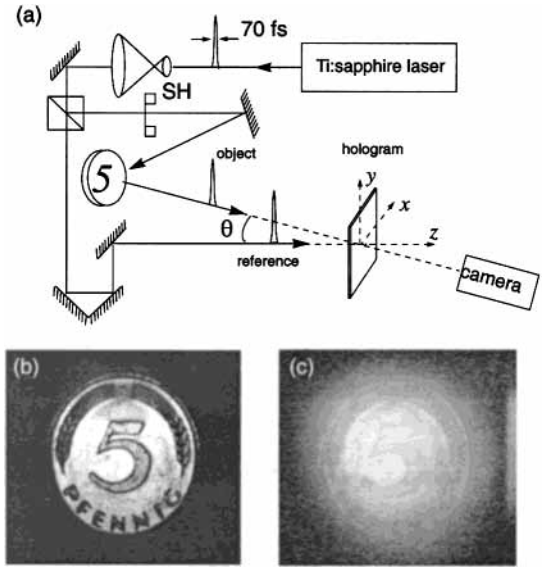

Figure 16. Experimental arrangement for writing holograms (a) with 70-fs-duration pulses, (b) original image, and (c) image produced from the hologram.

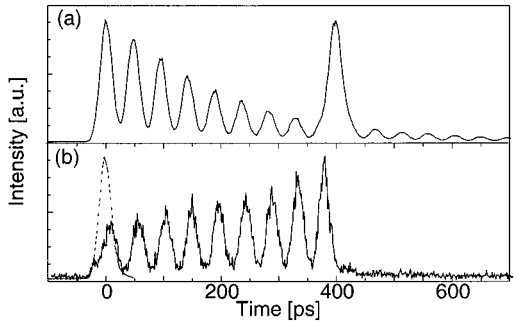

Figure 17. Time reversal by time-domain PSHB hologram.

distinguishes between what part of an object arrives before and what after the reference pulse. Recently, we have used this effect to study "time edge" holograms in which the direction of diffraction changes abruptly as a function of the delay[38] and have shown that such holograms can be used to measure the homogeneous spectrum of the chromophore molecules in a very short interval of time. Causality can be also used as a "time shutter" for viewing objects hidden behind an opaque screen.[39]

Figure 16 shows an experiment[40] in which we record an image of a coin illuminated with 70 fs duration pulses from a mode-locked Ti:sapphire laser. For this experiment, we use a 200-μm-thick polyvinylbutyral film activated with special phthalonaphthalocyanine dye molecules absorbing at the 750−780 nm wavelength of the Ti:sapphire laser. The solubility of these molecules in polymer was chemically enhanced by introducing the 2,4-dimethyl-3-pentoxy substituents. The sample was contained at temperature $T = 2$ K in an optical cryostat. It is significant that the illuminating light had a coherence length of only 20 μm, which was 2 orders of magnitude less than would be normally needed to record an image hologram. The time delay was $\Delta\tau \approx 100$ ps, which excludes any conventional interference between the beams. This experiment showed that high-resolution image holograms can be recorded even if the light shows no interference in the conventional sense—all of the interference occurs in the spectral dimension of the PSHB medium.

Figure 17 shows an experiment that illustrates the effect of inversion of the time shape of the object pulse. Trace a shows the writing object pulses consisting of a train of picosecond pulses, followed by a single reference pulse. The object pulse train starts at time $t = 0$ and extends over 1 ns, whereas the delay of the reference pulse is 400 ps. Trace b shows the signal obtained from the hologram in the conjugated diffraction direction. The hologram reproduces a time-inverted replica of that part of the object that preceded the reference during writing.

4.2. Associative Recall of Time-Space Events. Time-and-space-domain holograms can be recorded also in an associative manner, without using a separate reference pulse. In this case, the recollection of the information is performed by illumination with a selected fragment of the original object.[41] Figure 18a shows a beam of a picosecond laser that passes through a stack of optical delays of 0, 34, 68, and 102 ps. Subsequently, the beam scatters from a ground glass plate in the forward direction, reaching the SHB hologram plate inside a cryostat. The writing procedure was accomplished simply by illumination with the object beam, without using any special reference. The readout was performed by illuminating the hologram with a part of the attenuated object beam. Figure 18b shows the original spatial image of the object observed with a photographic camera and the corresponding temporal intensity profile measured with a picosecond time resolution streak camera. The arrows indicate which part of the object in the time-domain corresponded to which part of the spatial image. Figure 18c shows the result of associative read-out with an interrogating "key", which consisted of the three first pulses. The hologram recalls by association the image and the temporal shape of the missing fragment. However, if we used a "key" that was the last fragment, then the hologram did not play back any of the missing parts of the object. This demonstrates again that the causality-related "time arrow" depends on the relative time ordering of the illuminating light signals, which is prohibiting associative recall of those parts of the scene that are in time later than the "key" fragment. Gabor has pointed out early on that this property of time-domain holograms resembles the functioning of human memory.[42]

A digital version of associative PSHB memory was studied in ref 43. In this case, the holograms served as programmable multidimensional (spatial, frequency, and time dimension) interconnecting optical elements between arrays of digitally coded input and output signals. PSHB materials allow the increase of the dimensionality of optical interconnections and were used to implement error-corrective autoassociative memory in time and frequency dimension.

4.3. Spectral Programming of Femtosecond Pulses. In this experiment, we show that it is possible to produce arbitrary time-domain pulse shapes by using PSHB holograms synthesized in the frequency dimension.[44] We recorded a set of PSHB gratings at different frequencies with variable, predefined relative amplitudes and phases by using a narrow-band tunable laser. We then applied a short subpicosecond pulse to generate a photon echo signal and measured its intensity profile in time domain. As the tunable narrow-band laser, we utilized a dye laser with the line width of 0.5 cm^{-1}. The SHB material was chlorin (H_2-dihydroporphyrin) in PVB at temperature of 2 K. The maximum diffraction efficiency of the recorded gratings was on the order of 1%. The readout was carried out by 200-fs-duration white light continuum in the wavelength range 630−635 nm generated with the help of an amplified femtosecond Ti:sapphire laser system. The time profile of the hologram signal was measured by cross-correlation with Ti:sapphire laser pulses.

Figure 19 shows different pulse trains that were synthesized by this method. For each pulse train, a separate set of frequency-domain gratings was recorded according to a given calculated amplitude and phase algorithm. The measured duration of the

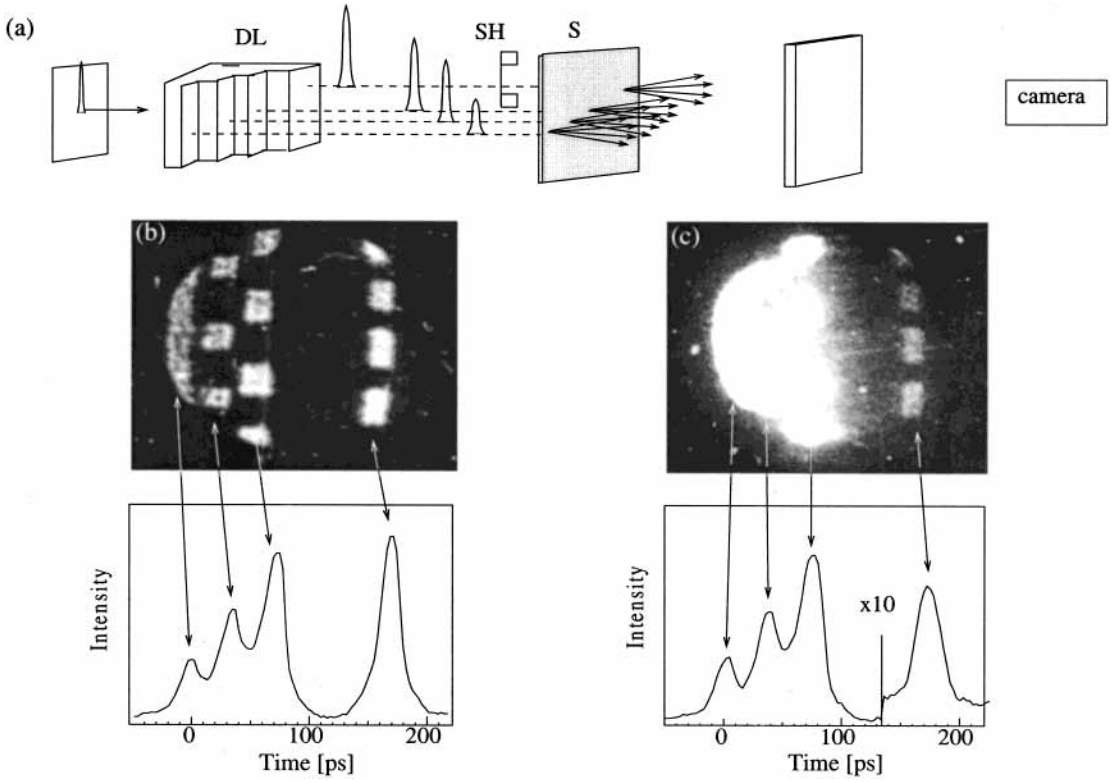

Figure 18. Associative recall of a time-and-space-domain event.

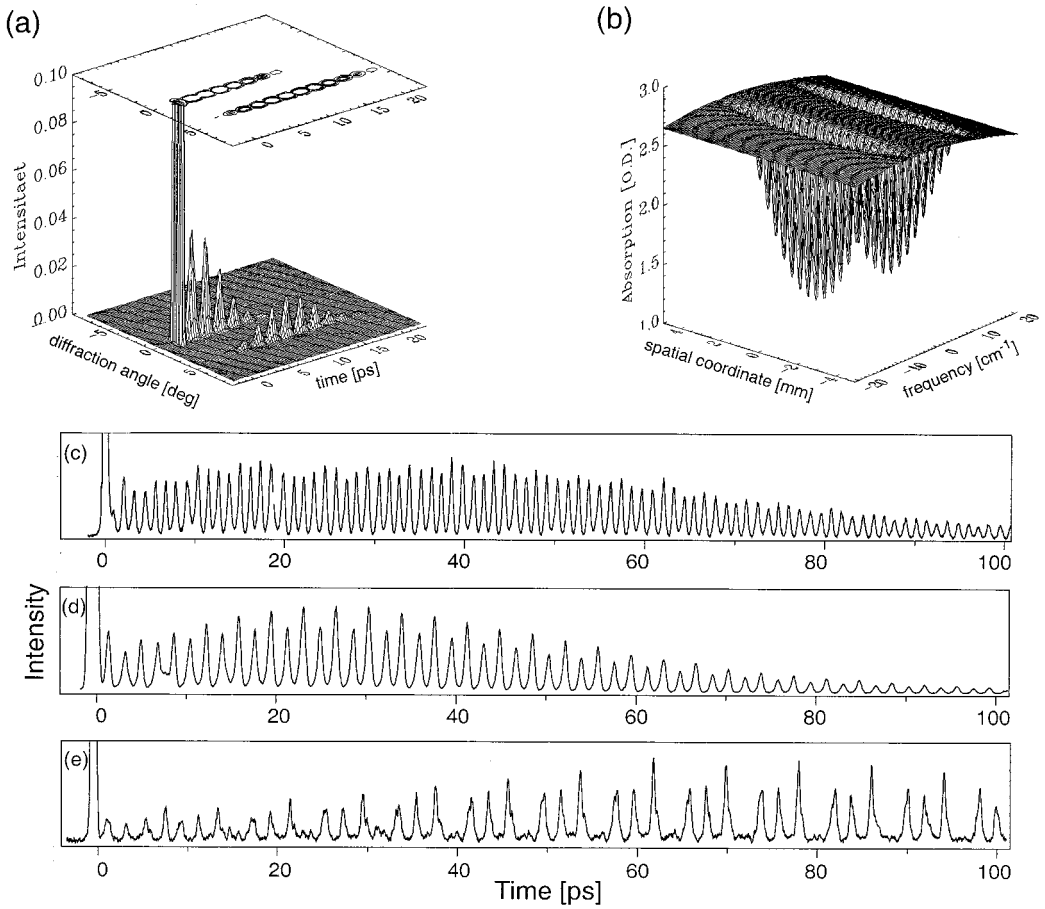

Figure 19. Spectrally programmed time-domain SHB holograms: (a) quasi-three-dimensional representation of one possible time-domain response function. The axis perpendicular to the time coordinate represents the diffraction angle. Panel b shows the calculated spatial-spectral structure that has to be written into the absorption spectrum of the SHB plate to produce the desired response function in the time domain; panels c−e show three different time response functions implemented in the experiment. The synthesized holograms are producing different series of subpicosecond pulses with predefined amplitudes and phases.

individual pulses in the train was about 350 fs, which gives the time resolution of the synthesized signals. The maximum time span of the pulse trains was about 0.5 ns and was limited by the finite homogeneous ZPL line width. The potential practical application of ultrafast synthesized pulse trains is in transmission and routing of data in optical fibers links and in ultrafast optical processors.

In all experiments described above, the recorded holograms are gradually erased by illumination with the read-out light. In certain applications such as permanent memories and pulse train generators, it is required that the recorded holograms are resistant with respect to irreversible erasure during the read-out. To resolve this problem, it is of great interest to use two-color photon-gated PSHB materials.[45] In these materials, permanent holes are produced only if an additional illuminating beam, typically of a different color or wavelength, is added. Read-out with only one color will not cause irreversible erasure. We have shown recently that photon-gated hole-burning allows practically nondestructive read-out of time-and-space-domain holograms.[46] It also allows read out of holograms with a much higher intensity than during the writing, without actually destroying the recorded information.

4.4. Time-Domain Holograms and Stark Effect. Earlier in this paper, we showed that Stark effect can be used to change the diffraction from narrow frequency-domain holograms. In this section, we will show how Stark effect changes the response of spectral holes in time domain. A simple qualitative explanation of anticipated effects may be given in terms of a spectral grating: because every narrow hole splits and broadens by the same amount, if the splitting becomes equal to half of the grating period, then the grating vanishes. Correspondingly, one may expect that the intensity of the time-domain response signal should also go to zero. With further increase of the Stark splitting, the contrast in the grating increases again and the time-domain signal should reappear again.

A quantitative consideration[47] yields that the time domain response function in an applied external electric field is given by

$$E^{\mathrm{Stark}}(t,x,y) = E^{\mathrm{out}}(t,x,y)G^{\mathrm{Stark}}(t,\vec{E}) \qquad (29)$$

where the time-domain function, G^{Stark}, is a characteristic of the molecular properties of the medium:

$$G^{\mathrm{Stark}}(t,\vec{E}) = \int_{\vec{\Omega}}(\vec{d}\vec{n})^4 \, \mathrm{e}^{-i2\pi\Delta\nu_{\mathrm{Stark}}(\vec{E},\,\vec{\Omega})t}\,\mathrm{d}\vec{\Omega} \qquad (30)$$

Here $\vec{d}$ is the optical transition dipole moment vector, $\vec{n}$ is the polarization vector of the optical field, and the integration is carried out over all solid angles and orientations. Function 30 depends on the static dipole properties of the impurity center and on the relative orientation of optical field polarization and the *E*-field vector but is universal in the sense that it does not depend either on the particular time profile (and spectrum) of the excitation pulses or on the width (and shape) of the homogeneous spectral line.

Let us note also that the external field does not alter the causality-related asymmetry of diffraction direction. Figure 20 shows an experiment demonstrating the effect of external electric field on a time-domain hologram comprising a train of picosecond pulses. During writing exposure, the voltage was zero. To generate an object pulse train (time delay between two adjacent pulses 120 ps), we used Fabry−Perot Etalon placed into the object beam before the cryostat. The time resolution is ∼30 ps, which is less than the actual duration of the laser pulses (<5 ps). When no voltage is applied during the read out, then

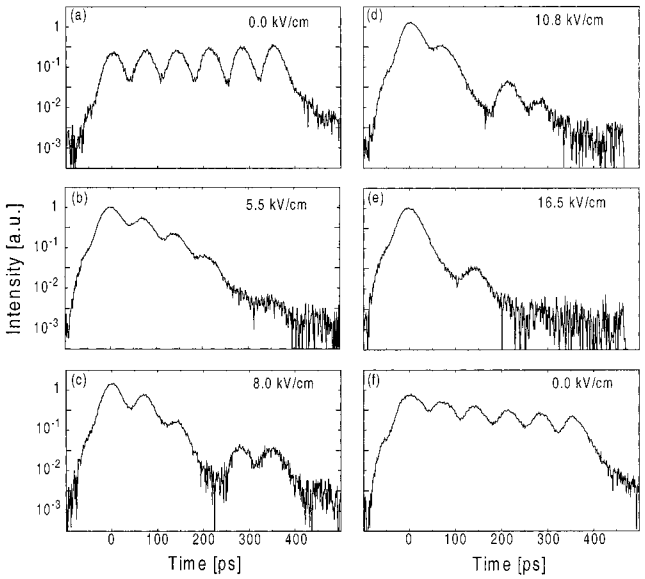

Figure 20. Time-domain response of a PSHB hologram at different applied electric field strength.

the hologram reproduces the time profile of the pulse train. When the voltage is applied, we observe that the shape of the time domain signal changes dramatically. The trace a was measured at zero voltage, the curves b−e are presented in the order of an increasing voltage (up to 16.5 kV cm^{-1}). The first pulse in the echo pulse train, which corresponds to a delay close to zero, exhibits almost no variation with the electric field. With all other pulses, however, we can clearly observe a dependence that resembles an oscillating function superimposed upon the original pulse train profile. The pulses with the largest delay are most sensitive to the applied voltage. We conclude that external electric field can be utilized to alter the time response of ultrafast holograms. Another application of this technique is measuring the static dipole moment of molecules using a broad-band laser source and a variable voltage source.

5. Summary

In summary, we have shown that light-sensitive materials, based on the effect of persistent spectral hole burning, can be used for recording of holograms with fascinating properties. Two different approaches to PSHB holography are described. In one case, the recording and readout of the holograms is performed by tuning a narrow line width laser in the frequency dimension. In the second case, these functions are accomplished in the time domian by using short pulses. In our discussions of PSHB holography, we have emphasized the intimate connection that exists between the time- and frequency-domain phenomena. The theoretical treatment that we have presented underlines common aspects of interference and diffraction in frequency-selective medium.

Advantages of PSHB come from the fact that high spectral selectivity is an intrinsic property of the recording material. We used this property to increase dramatically the number of image holograms recorded at one spatial location and showed that interference in the frequency dimension can be used to eliminate cross-talk between adjacent holograms. PSHB holography holds great promises for future generation ultrafast storage and processing devices. The special properties of PSHB open up principally new ways of recording and manipulating broad-band optical signals. The important fact is that the frequency selectivity is not restricted to any specific beam propagation

direction or spatial location. This allows us to speak about true multidimensional optical recording, where the spatial coordinates are fully independent from the frequency or time coordinate or both. Currently available organic PSHB materials such as dye-doped polymers provide at liquid helium temperature up to tens of thousands of frequency channels within inhomogeneous bandwidths of 5−10 THz. This matches well the bandwidth required for operation on a femtosecond time scale.

Acknowledgment. We are obliged to Dr. H. Wolleb and Dr. H. Spahni for providing phthalonaphthalocyanine compounds, to Dr. Ollikainen for participating in the experiments, and to Dr. Guido Grassi and Dr. Indrek Renge for chemical preparation of some of our samples. A part of this work was supported by Comission of Technology and Innovation (KTI), the Board of the Federal Institutes of Technology (FIT), and ETH Zurich, Switzerland. A. Rebane thanks AFOSR for support.

References and Notes

(1) Sincerbox, G., Ed. *Selected Papers on Holographic Storage*, SPIE Milestone Series, Vol. MS 95; SPIE Optical Engineering Press: Bellingham, WA, 1994.

(2) Longuet-Higgins, H. C. *Nature* **1968**, *217*, 104.

(3) Gorokhovskii, A. A.; Kaarli, R. K.; Rebane, L. A. *JETP Lett*. **1974**, *20*, 216. Kharlamov, B. M.; Personov, R. I.; Bykovskaya, L. A. *Opt. Commun*. **1974**, *12*, 191.

(4) Rebane, K. K. *Impurity Spectra of Solids*; Plenum Press: New York, London, 1970.

(5) Castro, G.; Haarer, D.; Macfarlane, R. M.; Trommsdorff, H. P. U.S. Patent 4,101,976, 1976.

(6) Rebane, A.; Kaarli, R.; Saari, P.; Anijalg, A.; Timpmann, K. *Opt. Commun*. **1983**, *47*, 173. Rebane, A.; Kaarli, R. *Chem. Phys. Lett*. **1983**, *101*, 279.

(7) Renn, A.; Meixner, A. J.; Wild, U. P.; Burkhalter, F. A. *Chem. Phys*. **1985**, *93*, 157.

(8) Kohler, B.; Bernet, S.; Renn, A.; Wild, U. P. *Opt. Lett*. **1993**, *18*, 2144.

(9) Hesselink, L.; Orlov, S. S.; Liu, A.; Akella, A.; Lande, D.; Neurgaonkar, R. R. *Science* **1998**, *282*, 1089.

(10) Meixner, A. J.; Renn, A.; Bucher, S. E.; Wild, U. P. *J. Phys. Chem*. **1986**, *90*, 6777.

(11) Mossberg, T. W. *Opt. Lett*. **1982**, *7*, 77.

(12) Saari, P.; Kaarli, R.; Rebane, A. *J. Opt. Soc. Am. B* **1986**, *3* (4), 527.

(13) Rebane, A.; Aaviksoo, J.; Kuhl, J. *Appl. Phys. Lett*. **1989**, *54*, 93.

(14) Schwoerer, H.; Erni, D.; Rebane, A. *J. Opt. Soc. Am. B* **1995**, *12*, 1083.

(15) Rebane, A.; Ollikainen, O. *Opt. Commun*. **1991**, *83*, 246.

(16) Ollikainen, O.; Rebane, A.; Rebane, K. *Opt. Quantum Electron*. **1993**, *25*, 569.

(17) Gygax, H. Dissertation ETH 10374, 1993.

(18) Huang, W.-Y.; Rebane, A.; Wild, U. P.; Johnson, L. W. *J. Lumin*. **1997**, *71*, 237−243.

(19) Altner, S. B.; Bernet, S.; Renn, A.; Maniloff, E. S.; Graff, F. R.; Wild, U. P. *Opt. Commun*. **1995**, *120*, 103.

(20) Holliday, K.; Croci, M.; Vauthey, E.; Wild, U. P. *Phys. Rev. B* **1993**, *47*, 14741.

(21) Holliday, K.; Wild, U. P. In *Molecular Luminescence Spectroscopy*; Schulman, S. G., Ed.; Chemical Analysis Series, Vol. 77; John Wiley: New York, 1993.

(22) Rebane, L. A.; Gorokhovski, A. A.; Kikas, J. V. *Appl. Phys. B* **1982**, *29*, 235.

(23) Wild, U. P.; Renn, A. *Mol. Cryst. Liq. Cryst*. **1990**, *183*, 119−129.

(24) Keller, C. U.; Graff, W.; Rosselet, A.; Gschwind, R.; Wild, U. P. *Astron. Astrophys*. **1994**, *289*, 41−42.

(25) Nussenzveig, H. M. *Causality and Dispersion Relations*; Academic Press: New York, 1972.

(26) Burkhalter, F. A.; Suter, G. W.; Wild, U. P.; Samoilenko, V. D.; Rasumova, V.; Personov, R. I. *Chem. Phys. Lett*. **1983**, *94*, 483−487.

(27) Maier, M. *Appl. Phys. B* **1986**, *41*, 73.

(28) Renn, A.; Meixner, A.; Wild, U. P. *J. Chem. Phys*. **1990**, *92*, 2748.

(29) Renn, A.; Meixner, A.; Wild, U. P. *J. Chem. Phys*. **1990**, *93*, 2299.

(30) Rebane, A.; Bernet, S.; Renn, A.; Wild, U. P. *Opt. Commun*. **1991**, *86*, 7.

(31) Bernet, S.; Kohler, B.; Rebane, A.; Renn, A.; Wild, U. P. *J. Lumin*. **1992**, *53*, 215−218.

(32) Bernet, S. Ph. D. Disseration, ETH Nr. 10292, 1993.

(33) Renn, A.; Wild, U. P. *Appl. Opt*. **1987**, *30*, 4040. De Caro, C.; Renn, A.; Wild, U. P. *Appl. Opt*. **1991**, *30*, 2890.

(34) Maniloff, E. S.; Altner, S. B.; Bernet, S.; Graf, F. R.; Renn, A.; Wild, U. P. *Appl. Opt*. **1995**, *34*, 4140.

(35) Plagemann, B.; Graf, F. R.; Altner, S. B.; Renn, A.; Wild, U. P. *Appl. Phys. Lett. B* **1998**, *66*, 67.

(36) Wild, U. P.; Renn, A.; DeCaro, C.; Bernet, S. *Appl. Opt*. **1990**, *29*, 4329.

(37) Saari, P.; Rebane, A. *Proc. Acad. Sci. Est. SSR Phys. Math*. **1984**, *33*, 322.

(38) Rebane, A.; Ollikainen, O.; Erni, D.; Schwoerer, H.; Wild, U. P. *J. Lumin*. **1995**, *64*, 283.

(39) Rebane, A.; Feinberg, J. *Nature* **1991**, *351*, 378.

(40) Rebane, A. Femtosecond Time-and-Space-Domain Holography. In *Trends in Optics, Research, Developments and Applications*; Consortini, A., Ed.; Academic Press: San Diego, CA, 1996; pp 165−188.

(41) Rebane, A. *Opt. Comm*. **1988**, *65*, 175.

(42) Gabor, D. *Nature* **1968**, *217*, 584, 1288.

(43) Rebane, A.; Ollikainen, O. *Opt. Commun*. **1991**, *83*, 246. Ollikainen, O.; Rebane, A.; Rebane, K. *Opt. Quantum Electron*. **1993**, *25*, 569.

(44) Schwoerer, H.; Erni, D.; Rebane, A.; Wild, U. P. *Opt. Commun*. **1994**, *107*, 123.

(45) Carter, T. P.; Bräuchle, C.; Lee, V. Y.; Manavi, M.; Moerner, W. E. *J. Chem. Phys*. **1987**, *91*, 3998.

(46) Rebane, A.; Reiss, D.; Renge, I.; Wild, U. P. *Chem. Phys. Lett*. **1996**, *262*, 155.

(47) Gygax, H.; Rebane, A.; Wild, U. P. *J. Opt. Soc. Am. B* **1993**, *10*, 1149.